MEMEA 2022, Conf MEMEA 2022, ConfID: 54994X

Terahertz Characterisation of Ordinary and Aggressive Types of Oral Squamous Cell Carcinoma as a Function of Cancer Stage and Treatment Efficiency

Shohreh Nourinovin, *Student Member, IEEE,* Muhammad M Rahman, Michael P Philpott, Qammer H. Abbasi, *Senior Member, IEEE,* Akram Alomainy, *Senior Member, IEEE,*

***Abstract*—Oral squamous cell carcinoma (OSCC) has asymptomatic characteristics that make it challenging to identify in the early stages and lead to metastatic effects. Terahertz (THz) spectroscopy and imaging are recognized as a novel technique for early cancer detection due to the non-ionizing nature and the significant THz wave absorption by water's hydrogen bonds and the higher hydration of tumours. Despite this potential, there is a lack of research on the THz characterisation of oral cancer with various essential biological conditions. THz characterisation based on frozen, freshly excised tissue restricts parametric studies on important components and diverse biological situations. Therefore, we cultivated the three-dimensional (3D), organotypic model of the OSCC, to investigate the THz spectroscopy of the tumour at various phases and the effects of the anticancer drug AG1478 on its THz spectra. Moreover, we have compared the characterisation of OSCC with two levels of aggressiveness and we contrasted how well the medication worked on these two types of cell lines. The measurements were performed at the frequency range of 0.4 to 1.6 THz, and with increasing malignancy of the samples, we observed higher refractive index, absorption coefficient, and complex permittivity than normal tissue. The results demonstrates that whereas AG1478 shifts the THz spectra in the direction of the normal tissue, it has no effect on aggressive OSCC (AOSCC) under the same circumstances. These findings may contribute to techniques that diagnose and detect tumours at the early stage.**

***Index Terms*—Terahertz spectroscopy, artificial tissue, oral squamous cell carcinoma, drug.**

I. Introduction

THZ wavelength is located between the microwave and the infrared region of the electromagnetic spectrum and is used in a wide range of industries, including product inspection, chemical and astronomical spectroscopy, and medical application [1]–[3]. THz spectroscopy and imaging have been widely employed in the medical area due to some advantages over conventional detection and diagnosis approaches. Compared with the higher frequency technologies, including computerized tomography (CT) scan, positron emission tomography (PET) scan, and X-ray, THz wavelength has lower photon energy and does not impose an ionization effect on the biological tissue. From a diagnostics perspective, a tumour biopsy is taken and histological slides are probed for various biomarkers. Biomarker detection mechanisms do not have enough resolution to distinguish the migrating cells, cancer tissue's border, and direction and need a large device or complicated pre-processing. It is also worth noting that cancer stem cells are transient with regards to their phenotype and for this reason, their biomarkers shift depending on their migratory state. A histologist is able to identify tumours by eye but without reliable biomarker staining, it is difficult to comment on the potential invasion profile of the tumour unless the tumour island itself has very distinctive characteristics. An example is the identification of individual cells migrating towards blood vessels as these cells can significantly affect mortality. On the other side, unlike optical frequencies, water exhibits strong absorption at the THz band, and therefore, cells and tissues with various hydration levels can reflect distinctive responses to THz radiation. This feature makes THz technology attractive for monitoring and detecting different types of tumours since malignant tissue has accumulated different water portions than healthy cells.

THz imaging, spectroscopy, and biosensors have all been investigated as early cancer detection tools. By highlighting the borders of the tumour, THz imaging [4] can assist surgeons in removing tumours. THz wave penetration into the human body is severely limited by water absorption, which concentrates THz imaging mostly on excised tissue. On the other hand, THz spectroscopy [5] can be used for less complex, inexpensive, and precise identification of biomarkers and malignancies. To increase the sensitivity, THz spectroscopy can also be used in conjunction with electromagnetic biosensors, such as THz metamaterials and metasurfaces [6]–[8].

Different types of cancers, have been studied with THz spectroscopy including breast [9], colon [10], gastric [11], skin [12]–[14], and oral cancer [6].

Oral cancer has a high mortality rate because of the soaring rate of metastasis to other body organs. Due to its asymptomatic attributes, oral cancer cannot be readily identified in its early stages. It can be developed in any part of the inner mouth (oral cavity), including the gums, tongue, the inner lining of

Sh.Nourinovin and A.Alomainy are with the School of Electronic Engineering and Computer Science, Queen Mary University of London, London E1 4FZ, U.K. (e-mail:s.nourinovin@qmul.ac.uk; a.alomainy@qmul.ac.uk), M.M.Rahman and M.P.Philpott are with the Centre for Cell Biology and Cutaneous Research of Blizard Institute, Queen Mary University of London, London E1 2AT, U.K. (e-mail: m.m.rahman@qmul.ac.uk; m.p.philpott@qmul.ac.uk), Q.H.Abbasi is with the James Watt School of Engineering, University of Glasgow, Glasgow, G12 8QQ, U.K. and the School of Electronic Engineering and Computer Science, Queen Mary University of London, London E1 4FZ, U.K. (e-mail: Qammer.Abbasi@glasgow.ac.uk)

MEMEA 2022, Conf MEMEA 2022, ConfID: 54994X

the cheeks, the roof of the mouth, and the mouth's floor (under the tongue). Oral squamous cell carcinoma (OSCC) makes up more than 90% of malignancies that develop in the mouth. Squamous cells, which are flat and look like fish scales when viewed via a microscope, cover the throat and mouth. When some squamous cells mutate improperly, squamous cell cancer develops. Despite its importance, only a small number of research studies have examined the characterisation of OSCC with THz spectroscopy [15], THz imaging [16]–[18] and THz metamaterials [19]–[22].

When using freshly excised oral cancer tissue for THz spectroscopy and imaging [23], [24], the sample faces a quick deterioration rate. It should be frozen as soon as collected, requiring the freezing equipment to be near the surgery site. Storage and specialized equipment raise the cost and complexity tremendously. Additionaly, this method increases the possibility of tissue damage from the freezing and thawing process leading to inaccurate results.

On the other hand, the intricate structure of biological tissues makes it difficult to distinguish between cancerous and healthy tissues. Removing tumours with the correct margins has a high error rate. Furthermore, the research of the behavior of cancer cells and the creation of effective pharmaceutical techniques rely on the parametric analysis of variables that are fixed in natural samples. In order to improve the accuracy of both tumour characterisation and margin discrimination, it is crucial to investigate the impact of various factors, such as cancer stage, therapeutic effectiveness, and variations in tissue cells, on the electromagnetic properties.

Skin equivalents are artificially reconstructed and consist of epidermal and dermal layers. These models can be created from primary cells and mimic genuine skin. The organotypic cell culture technique has aided in advancing cancer research and drug discovery during the past ten years. Although it is possible to culture cells in 2D monolayers, more modern organotypic cell culture technology that uses 3D gel-based techniques enables more sophisticated studies that more accurately mimic the appearance of skin. Compared to 2D culture, 3D tissues provide more precise information on tumour features and therapeutic efficiency since they are morphologically and physiologically more similar to an in vivo environment [25].

Current research works are mainly based on freshly excised oral tissue, and they have rarely been explored based on organotypic models [26] [27]. Tianmiao et .al [27] proposed an oral cancer phantom without water content by applying graphite powders into a polyvinyl chloride plastisol matrix to study the THz optical properties.

Aside from the significance of early cancer identification, monitoring the cancer stage and creating novel anticancer medications with multi-target behavior may lead to increased efficacy, fewer instances of acquired resistance, and fewer adverse drug reactions in patients [28]. The research on how different medications affect tumour cells makes diagnosing different types of tumours easier and offers comprehensive knowledge of the diagnostic procedure. Therefore, more in-depth knowledge of drug-target interactions and their receptors is required to develop improved therapeutic techniques. The current study was motivated by the fact that to our knowledge, very few research papers have considered the relationship between cancer stage and interaction of THz waves with anticancer drugs, aside from the rare research effort on oral and especially aggressive oral cancer [22], [29], [30]. Moreover, if we are able to fully characterise OSCC cancer cells with THz spectroscopy, we would be able to identify the individual cancer cells and possibly count the number of these cells in a biopsy to give an indicator of tumour aggressiveness. This could also be used alongside histological staining where there could be selective staining of tumours if the histologist has a better indication of the tumour characteristics identified by THz spectroscopy.

In this study which is the extension of the previous result presented in [6], we investigated the impact of two tumour suppression phases compared with normal skin and the effect of anticancer treatment on its THz electromagnetic characteristics using the 3D organotypic model of ordinary and aggressive types of OSCC. 3D culture system is designed to better represent tumours in vivo, and practically more in line with tumour biopsies. In 2D culture as explored in most studies, tumour cells are difficult to characterise with THz spectroscopy. In our model, we consider the 3D behaviour of the tumour cells. Normal epithelial cells will form layers of cells and bind tightly together, only cancer cells will become invasive and form independent tumour islands away from the epithelial layers. With the advantages offered by THz spectroscopy, we investigated the cancer cells for their unique behaviour in 3D culture. Several samples were cultivated, and their THz characterisation was explored using the terahertz time-domain spectroscopy system (THz-TDS) in transmission mode. Section II presents the cultivation process of the 3D organotypic model of the samples. Section III details the experiment's technique and THz-TDS configurations. Consequently, section IV explains calculations for extracting optical parameters. The findings of characterizing normal tissue, ordinary and AOSCC with two distinct levels of cell growth, and treated samples with AG1478 medication are shown in Section V. Finally a summary of covered discussion proposed in Section VI.

II. Sample Preparation

The biology of OSCC appearance along with molecular biology of oral tissue is illustrated in Fig. 1

Fig. 2 shows the 3D organotypic skin cell cultivation procedure. The dermis layer is developed on porous filters inside transwell inserts using fibroblasts grown in a collagen matrix. Keratinocytes are planted on top of the dermis layer after one week. After another week, the gels are taken out, removing the keratinocyte layer's contact with the culture medium and establishing the air-liquid interface necessary for keratinocyte differentiation and stratification of the epithelial layer. The epidermal layer can be taken 1-2 weeks after the air-liquid interface is formed and becomes clearly opaque as the culture matures.

In our experiment, NEB1 normal dermal keratinocytes have been used for control along with immortalized OSCC cell lines of CA1 and LUC4 for an ordinary and aggressive type of OSCC.

MEMEA 2022, Conf MEMEA 2022, ConfID: 54994X

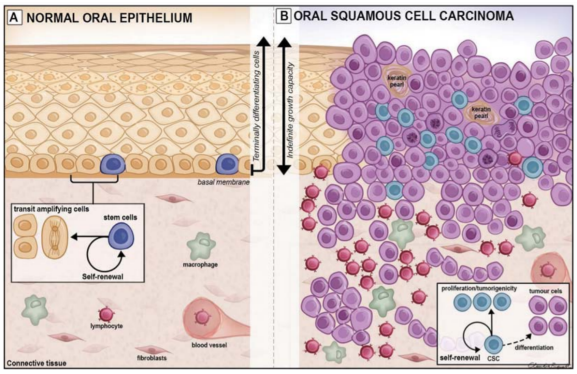

Fig. 1: Biology of healthy oral tissue and OSCC tissue. This figure is adapted from [31] with permission from the copyright owner.

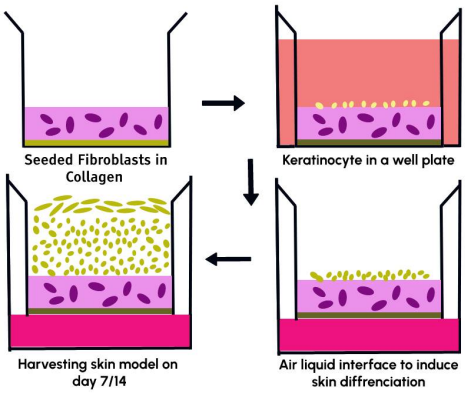

Fig. 2: Different stages of 3D organotypic cell culture

Also, the EGFR inhibitor AG1478 used as the anticancer drug [32], [33]. Each gel contains 500,000 fibroblasts mixed into 200 μl collagen type I, 200 μl of growth factor reduced Matrigel (Corning) and 50,000 keratinocytes seeded on top of the dermis gel layer.

All cells were cultured in DMEM/Ham's F12 (Gibco) supplemented with 10% (v/v) heat-inactivated foetal bovine serum (FBS) (Lonza), 2% (v/v) penicillin-streptomycin (PAA Laboratories), 2 nM L-glutamine and RM+ supplement containing 0.5 μg/ml hydrocortisone, 5 μg/ml insulin, 10 ng/ml epidermal growth factor (EGF), 5 μg/ml transferrin, 9.2x10-4 M liothyronine and 1x10-10 M cholera toxin (Sigma). Initial dermal fibroblasts were grown in the same medium. The gels were harvested one or two weeks after the keratinocytes were sown on top of the 3D gels. The samples were treated with AG1478 for 72 hours.

Finally, the cultivated tissues were classified into seven groups of 2 weeks normal skin, 1 and 2 weeks OSCC and AOSCC, treated OSCC and AOSCC as presented in Table.I.Between these time points and particularly for 3D cultures, OSCC cell lines form tumour islands and the most invasive cells invade deep into the gel. In the context of CA1 and LUC4 OSCC cell lines, CA1 cells produce spherical tumour islands whereas, LUC4 cells form fewer tumour islands but invade considerably deeper into the gel compared to CA1 cells. We expected and found differences between the two time points. Between the two stages, the second time point will have more tumour cells (and migratory cells) present, further developed tumour islands, and a more developed tumour microenvironment. With this system, we can investigate a number of characteristics that are relevant to oral tumours in vivo.

A sample of OSCC tissue kept in phosphate-buffered saline (PBS) with a side, and front view is illustrated in Fig.3.

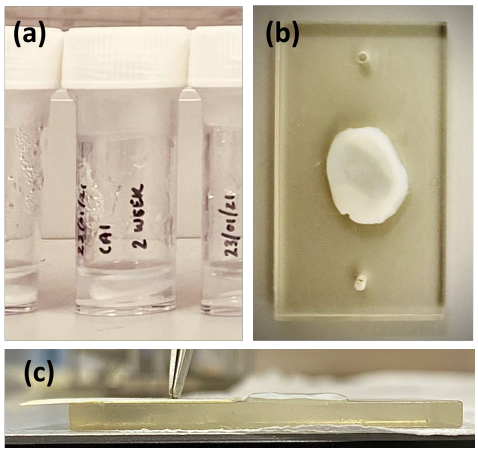

Fig. 3: Cultivated 3D organotypic model (a) samples kept in PBS with (b) front and (c) side view in Centre for Cell Biology and Cutaneous Research of Blizard Institute, Queen Mary University of London.

III. Experiment Methods

THz-TDS in transmission mode was used to assess the optical parameters. As many dielectric materials have their spectral fingerprints in the THz frequency region, THz-TDS can be used to examine and separate diverse biological samples. It has a coherent synchronized source and detector that delivers instant time domain amplitude measurement of the THz waves. THz time-domain data takes a single pulse, with a period of 1 ps, followed by a series of attenuated pulses originating from reflections at the interface of components within the THz-TDS system or from etalon reflections within the sample itself. To analyse the electromagnetic characteristics, THz transmission amplitudes of the samples were measured. For the experiment, the pulses generated by a 780 nm femtosecond Ti: sapphire laser were divided into the pump and probe beams using a beam splitter. A mechanical delay stage provided a time delay between two beams. To produce THz waves, the pump beam was focused onto a low-temperature-grown GaAs photoconductive antenna. To measure the THz transmission, generated THz waves were collimated and then focussed into the sample loading region. The generated THz wave goes through the sample and overlaps with the probe beam in a ZNTe crystal, allowing enough interaction length of the probe beam and THz wave. Finally, by catching orthogonally polarized parts of the probe beam, the THz waves were recorded using a lock-in amplifier that locks and records the detected THz data by a computer-generated program.

MEMEA 2022, Conf MEMEA 2022, ConfID: 54994X

To ensure accuracy and comparability, each sample was treated by soaking in ethanol to remove PBS residue. Then, a caliper was used to estimate the thickness of the tissue sample. Next, each sample was placed between two TPX plates with 300 μm spacers (equal to sample thickness) in a sample holder (as illustarted in Fig. 4). This ensures that the thickness remains relatively consistent across the entire surface. The TPX plates have a low absorption coefficient of less than 1 cm^{-1}, a refractive index of 1.46, and exhibit non-dispersive behavior in the THz frequency range of 0.1 to 3 THz. Therefore, for each sample, the reference signal was determined by measuring the transmitted signal through the TPX plates. Consequently, the reference signal was recorded first, followed by recording the time domain data of each sample individually as they were placed in the sample holder perpendicular to the THz wave. The experiment was conducted under controlled conditions, with measurements taken three times on each sample in different locations. The measurements carried out for all seven types of sample (Table. I) with same mentioned protocol. After recording the time domain amplitude and phase of each sample, a fast Fourier transform was then used to analyze the signal and extract electromagnetic parameters, such as the refractive index, absorption coefficient, and real and imaginary components of permittivity. To reduce non-linear distortion of THz waves at higher frequencies, the operation frequency was limited to between 0.4 and 1.6 THz. These calculations will be discussed in section IV to further elaborate on the findings.

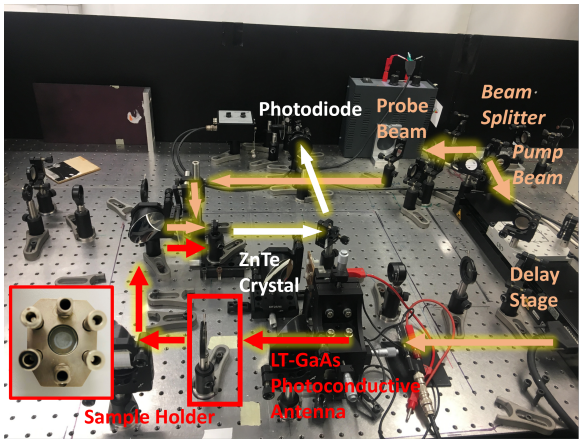

Fig. 4: THz-TDS in transmission mode along with the sample holder perpendicular to the incident THz wave.

IV. Electromagnetic Parameter's Processing

The raw taken results were time-domain electric field signal, and for calculation of the electromagnetic parameters, a fast Fourier transform was used to extract the amplitude and phase of the THz signal.

Due to the thin-film nature of biological samples, they are robustly influenced by multiple reflections inside the sample, the so-called Fabry-Perot effect. This phenomenon was also considered in signal processing with an iterative fitting process based on the polynomial fit of the electromagnetic parameters. The complex measured transfer function is :

$$H_e(f) = \frac{E_{sample}(f)}{E_{ref}(f)} \tag{1}$$

Where $E_{sample}(f)$ and $E_{ref}(f)$ are the complex spectra of the sample and reference respectively.

The refractive index of n_s, extinction coefficient of κ_s and absorption coefficient of α_s were calculated according to below equation:

$$n_s(f) = n_0 - \frac{c}{2\pi f d}(\Phi_{sample}(f) - \Phi_{ref}(f)) \tag{2}$$

in which $\Phi_{sample}(f)$ and $\Phi_{ref}(f)$ are the the measured transmission's phase coefficient for the sample and reference signals, c is the speed of light in vacuum, d is the sample thickness, and n_0 and $\hat{n}_s$ are the complex refractive index of air and sample, respectively.

$$\kappa_s(f) = \frac{-c}{2\pi f d} ln(|H_e(f)| \frac{4\hat{n}_s(f)n_0}{(\hat{n}_s(f)+n_0)^2}) \tag{3}$$

$$\alpha_s(f) = \frac{4\pi f}{c}\kappa_s(f) \tag{4}$$

Consequently, the relative complex permittivity can be calculated by Eq.5 with the real and imaginary components represented by Eq.6:

$$\hat{\epsilon}(f) = (n_s(f) - jk_s(f))^2 \tag{5}$$

$$\epsilon'(f) = n_s(f)^2 - k_s(f)^2, \epsilon''(f) = 2n_s(f)k_s(f) \tag{6}$$

Finally, the means and standard deviations for each sample's measurements were determined.

V. Results and Discussion

The THz time-domain waveforms of the healthy oral tissue and reference signal are shown in Fig. 5. Compared to the reference, it is evident that the THz pulse was affected after passing through the tissue. The pulses transmitted through the sample were delayed more than the reference, indicating a higher sample refractive index than the reference. The peaks of the electric field for the sample were also decreased, proving the tissue sample's energy absorption. These results confirm that biological tissues typically have a higher refractive index and more substantial THz absorption coefficient.

A. Impact of stage and malignancy degree of the oral cancer on the THz spectra

Fig. 6 and Fig. 7 show the refractive index, absorption coefficient and real and imaginary permittivity of cultivated 3D organotypic models of normal, OSCC and AOSCC tissues with tumour suppression phase of one and two weeks.

Regarding normal tissue, the refractive index is recorded between 1.47 and 1.35, while the absorption coefficient rises from near 17.33 to 78.06 cm^{-1}. Also, the extracted real and imaginary permittivity from Eq.6, calculated around 2 and 0.3, respectively. According to Fig. 6, the corresponding refractive index, absorption coefficient, and real and imaginary

MEMEA 2022, Conf MEMEA 2022, ConfID: 54994X

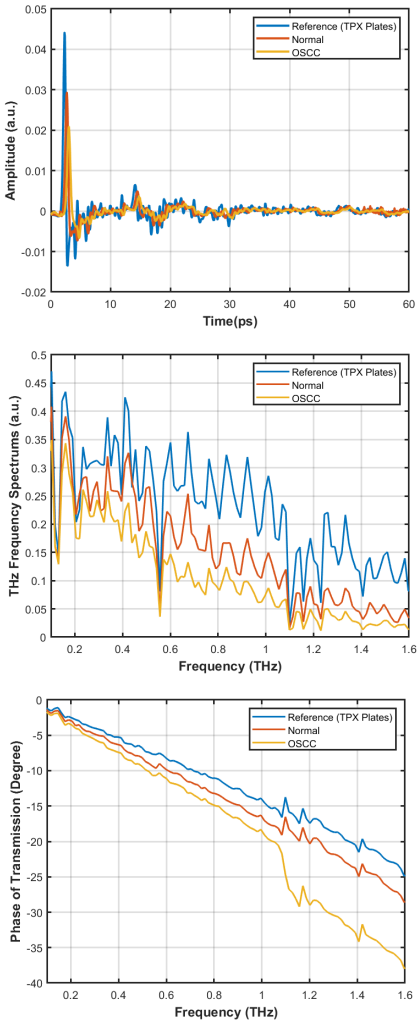

Fig. 5: (a) Typical THz time-domain electric field signals for a healthy oral tissue and reference signal through TPX plates. (b)-(c) corresponding FFT amplitude and phase.

permittivity go substantially higher than the healthy sample in the band of 0.4 to 1.6 THz when the normal tissue is replaced with the OSCC of a 1-week suppression phase. From a biological standpoint, malignant tissue has less room for lattice contraction, which results in less water being drawn from cancerous cells during the contraction process. On the other hand, water builds up because of the accelerated proliferation of vessels around malignant cells. This has also been looked at in [34] which justifies the higher hydration of cancer cells as an acceleration mechanism of their respiration rate and their capacity to compete with non-malignant cells for nutrition.In a recent study, the intracellular water variation was also examined in the transformation of normal breast tissue into malignant breast tissue, and it was discovered that there was an enhanced rotational motion of water around the cells ([35]).

Increasing the degree of carcinogenesis has been explored by measuring the spectra of the two weeks OSCC samples. The results of presented parameters in Fig. 6, exhibit more surge in both the refractive index and absorption coefficient. The outcome confirms that the progressive rise in cell hydration induced by successive cancer mutations is the basic mechanism of carcinogenesis, and the degree of malignancy increment with the degree of cell hydration.

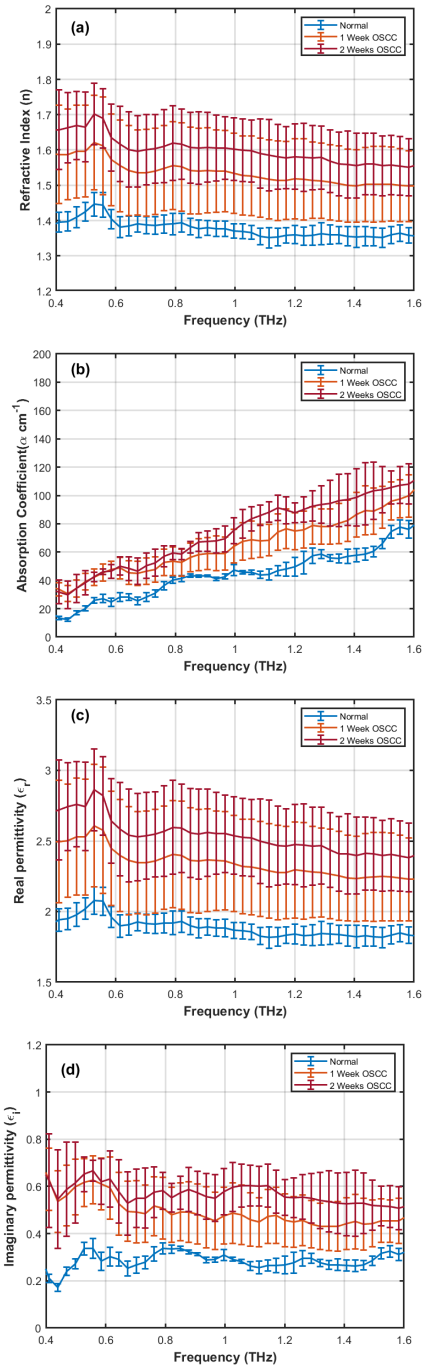

Fig. 6: THz spectra of 3D organotypic models of normal oral tissue and OSCC with tumour suppression phase of 1 and 2 weeks (a) refractive index, (b) absorption coefficient, (c) real part of permittivity (d) imaginary part of permittivity.

The obtained results are compatible with the previous research works in THz characterisation of OSCC in ref [15] which demonstrated the higher water absorption of OSCC in a freshly excised tissue. A very recent research work [36]

MEMEA 2022, Conf MEMEA 2022, ConfID: 54994X

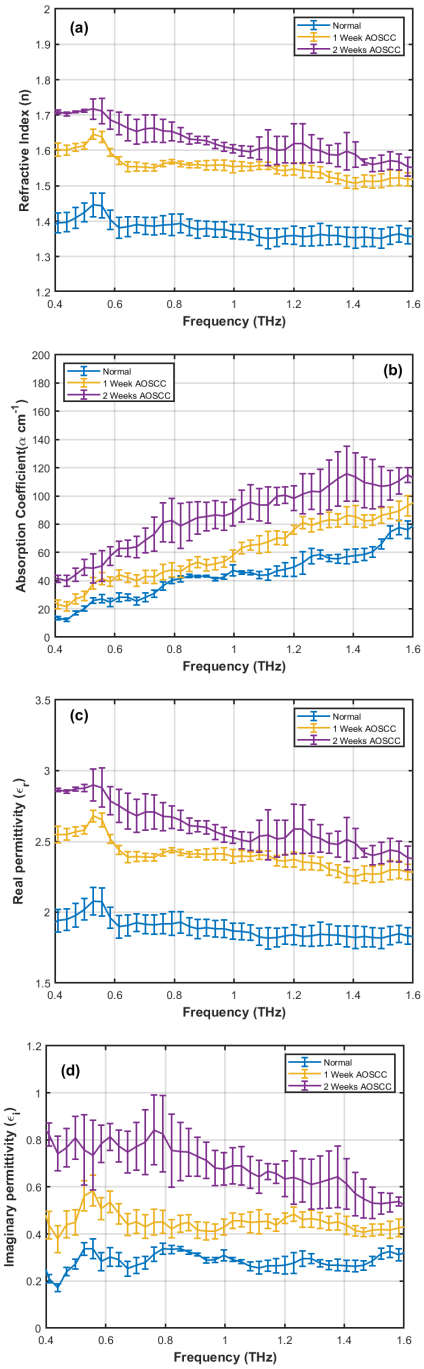

Fig. 7: THz spectra of 3D organotypic models of normal oral tissue and AOSCC with tumour suppression phase of 1 and 2 weeks (a) refractive index, (b) absorption coefficient, (c) real part of permittivity (d) imaginary part of permittivity.

also studied the formalin-fixed natural OSCC compared with ameloblastoma (benign) and odontogenic keratocyst tissues using pulsed terahertz reflection spectroscopy technique and observed higher refractive index and absorption coefficient for oral cancer. THz characterisation of SCC cells in skin tissue is also investigated in ref [37], which confirms a lower reflection and higher absorption of the tumour from the healthy cells.

In order to further explore the impact of malignancy degree in the THz spectra, we have calculated the same parameters for 1 and 2 weeks AOSCC. In fact, we have characterized OSCC cell lines with different levels of aggressiveness based on the percentage of epithelial-to-mesenchymal transitioning (EMT) cells. These cell lines also have different 3D culture phenotypes, and then we were interested in observing the difference with the ordinary OSCC. According to Fig. 7, the spectra of the AOSCC for both refractive index and absorption coefficient are somehow higher than the other type of studied OSCC for both one week and two weeks tumour suppression phase. For the two weeks AOSCC, the refractive index starts from 1.7 at the frequency of 0.4 THz and falls to near 1.55, while in the case of the previous studied OSCC, it begins at a point lower than 1.7 at 0.4 THz and gradually declines toward 1.6 THz. The same behaviour can be seen for the absorption coefficient spectra with a start point of 40 cm^{-1} at 0.4 THz to near 120 cm^{-1} at 1.6 THz. Although for the ordinary type of OSCC, it begins at a point lower than 40 cm^{-1} and ends at points near 110 cm^{-1}. The same trend can also be seen for calculated real and imaginary parts of permittivity.

B. Impact of treatment with the anticancer drug on the THz spectra

Epidermal growth factor (EGF) is responsible for the proliferation of SCC, and EGF receptor (EGFR) contributes to tumour growth. Along with the conventional anticancer drugs, agents that stop EGFR may lead to inhibit proliferation and induce apoptosis in SCC cells. AG1478 is a specific EGFR inhibiator and block tumour cell from growth, migration, and invasion. Sayaka et al. [38] investigated using the AG1478 with the conventional anticancer drug cisplatin on the OSCC cell lines and concluded that EGFR inhibitors might represent a proper approach for overcoming resistance to cisplatin-mediated apoptosis. Same results have been reported in [39] for OSCC and lung cancer [40] as well.

Fig. 8 represents the THz characterisation of the treated OSCC samples with AG1478 for 72 hours compared to the two weeks OSCC and normal tissue. According to Fig. 8.a, the refractive index of the treated samples declines from 1.65 to 1.47 at 0.4 THz and 1.55 to 1.36 at 1.6 THz for two weeks OSCC and treated sample, respectively. Fig. 8. (b-d) also shows same decreasing trend for absorption coefficient and complex permittivity of the treated samples compared to the two weeks OSCC. According to our expectations, these results show the fall of the THz spectra for the treated tissue toward healthy sample. Besides, one hypothesis also could be related to the drug's effect on the hydration level of tumour cells. Marquest et al. [28], [41] investigated the effect of cisplatin and Pt2Spm drugs on breast and bone cancers and confirmed a direct effect of the anticancer drug on the intramolecular water characteristic of treated tissue with inelastic and quasi-elastic neutron scattering techniques. They observed that adding concentrations of cisplatin changes the characteristic structure of intracellular water and causes reduced mobility of intracellular water. This outcome emphasizes the significance of intracellular water mobility as a promising target of anticancer agents [28]. These examinations may comply with the presented

MEMEA 2022, Conf MEMEA 2022, ConfID: 54994X

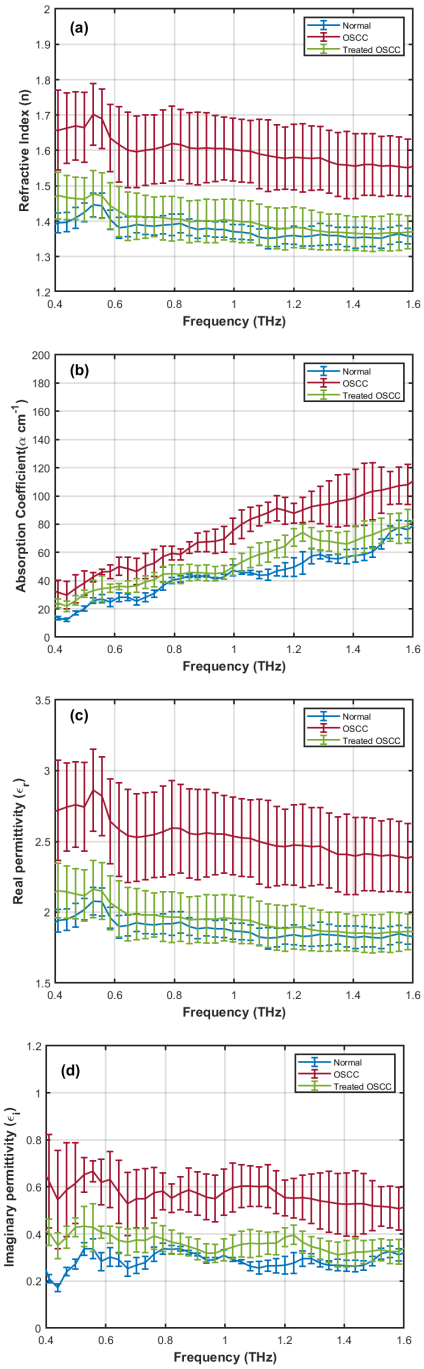

Fig. 8: THz spectra of 3D organotypic models of normal oral tissue, 2 weeks OSCC and 72 hours treated samples with AG1478 drug (a) refractive index, (b) absorption coefficient, (c) real part of permittivity (d) imaginary part of permittivity

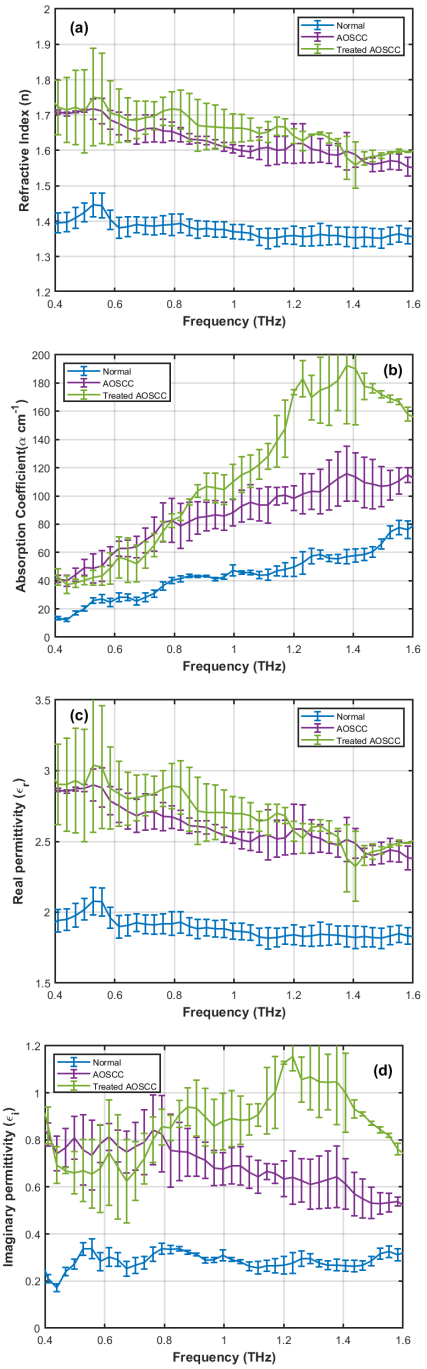

Fig. 9: THz spectra of 3D organotypic models of normal oral tissue, 2 weeks AOSCC and 72 hours treated samples with AG1478 drug (a) refractive index, (b) absorption coefficient, (c) real part of permittivity (d) imaginary part of permittivity

results and the hydration level changes of the cultivated tissues imposed by the drug. To go one step further with exploring the effect of the drug on the THz spectra, we have also treated the 2 weeks aggressive type of OSCC with AG1478 for 72 hours and the results of the refractive index, absorption coefficient and real and imaginary parts of the permittivity is presented in Fig. 9.(a-d). As can be shown, not only the refractive index and absorption coefficient of the treated AOSCC is not reduced in comparison with the two weeks ordinary OSCC, but also there is a slight rise. The result contradicted with what we observed for the non-aggressive type of OSCC (Fig. 8) in which the treatment made a fall in both the refractive index and absorption coefficient. While we don't observe an increase in cell death, there is a considerable effect on cell morphology. CA1 cells produce smaller tumour islands and LUC4 are restricted in their invasion and migration. This finding may

MEMEA 2022, Conf MEMEA 2022, ConfID: 54994X

TABLE I: Extracted refractive index (n), absorption coefficient (α), real permittivity (ϵ_r) and imaginary permittivity (ϵ_i) for all types of cultivated organotypic samples corresponding to the frequency range of 0.4-1.6 THz

Sample Type	$f(THz)$	n	$\alpha(cm^{-1})$	ϵ_r	ϵ_i
2 weeks normal tissue	(0.4-1.6)	(1.39,1.35)	(13.33,76.04)	(1.94,1.83)	(0.21,0.31)
1 week OSCC	(0.4,1.6)	(1.58,1.49)	(29.77,99.71)	(2.49,2.22)	(0.62,0.45)
2 weeks OSCC	(0.4,1.6)	(1.65,1.55)	(30.01,108.14)	(2.71,2.38)	(0.62,0.50)
Treated 2 weeks OSCC under 72 hours	(0.4,1.6)	(1.47,1.36)	(23.74,78.62)	(2.15,1.86)	(0.42,0.32)
1 week AOSCC	(0.4,1.6)	(1.60,1.51)	(23.09,93.10)	(2.54,2.28)	(0.43,0.42)
2 weeks AOSCC	(0.4,1.6)	(1.70,1.55)	(41.25,114.85)	(2.86,2.38)	(0.82,0.53)
Treated 2 weeks AOSCC under 72 hours	(0.4,1.6)	(1.72,1.59)	(42.70,157.94)	(2.90,2.48)	(0.86,0.76)

indicate that AG1478 under the same condition is less effective against AOSCC.

The results and comparison between the extracted electromagnetic parameters for all types of samples are summarized in Table. I. These observations and measurements may help understand the drug-tissue interaction and help to develop multi-target anticancer medications.

VI. Conclusion

The current study examines the THz characterisation of cultivated 3D organotypic models of OSCC with two levels of aggressiveness (CA1 and LUC4 cell lines), and it presents a new set of info on how THz waves interact with OSCC at various stages of the disease as well as the effectiveness of the anticancer drug AG1478. The corresponding refractive index, absorption coefficient, and complex permittivity of the cultured samples were extracted and compared based on measurements made with THz-TDS in the frequency range of 0.4 to 1.6 THz. The findings show that the tumour's refractive index and absorption coefficient are larger than those of normal tissue for both types of ordinary and AOSCC, which is consistent with the previous study. Additionally, it is shown that as malignancy levels grow, all electromagnetic parameters likewise increase. The tumour cells' increased hydration and increased THz wave absorption are related to these alterations. According to the observations for treated OSCC with EGFR inhibitor of AG1478, it is assumed that the medication with the same condition does not work for AOSCC because the retrieved optical characteristics of the treated ordinary type of OSCC fall toward the normal sample, but it is the opposite for treated AOSCC. These findings could help advance the OSCC treatment at an early stage, assist with multi-target pharmacological strategies, and a step toward creating more efficient OSCC treatments.

Acknowledgment

This research was supported by the School of EECS and Centre for Cell Biology and Cutaneous Research of Bilzard Institute at the Queen Mary University of London and James Watt School of Engineering, University of Glasgow.

References

[1] D. Fan, A. Ren, N. Zhao, D. Haider, X. Yang, and J. Tian, "Small-scale perception in medical body area networks," *IEEE journal of translational engineering in health and medicine*, vol. 7, pp. 1–11, 2019.

[2] J.-H. Son, S. J. Oh, and H. Cheon, "Potential clinical applications of terahertz radiation," *Journal of Applied Physics*, vol. 125, no. 19, p. 190901, 2019.

[3] A. al Abohmra, H. T. Abbas, M. S. Rabbani, C. Li, A. Alomainy, M. Imran, Q. H. Abbasi *et al.*, "An ultrawideband microfabricated gold-based antenna array for terahertz communication," *IEEE Antennas and Wireless Propagation Letters*, 2021.

[4] M. El-Shenawee, N. Vohra, T. Bowman, and K. Bailey, "Cancer detection in excised breast tumors using terahertz imaging and spectroscopy," *Biomedical Spectroscopy and Imaging*, vol. 8, no. 1-2, pp. 1–9, 2019.

[5] Y. Peng, C. Shi, X. Wu, Y. Zhu, and S. Zhuang, "Terahertz imaging and spectroscopy in cancer diagnostics: a technical review," *BME Frontiers*, vol. 2020, pp. 1–11, 2020.

[6] S. Nourinovin, M. M. Rahman, M. P. Philpott, and A. Alomainy, "Terahertz characterisation of artificially cultured oral cancer with stem cell lines for healthcare applications," in *2022 IEEE International Symposium on Medical Measurements and Applications (MeMeA)*. IEEE, 2022, pp. 1–5.

[7] M. Beruete and I. Jáuregui-López, "Terahertz sensing based on metasurfaces," *Advanced Optical Materials*, vol. 8, no. 3, p. 1900721, 2020.

[8] S. Nourinovin and A. Alomainy, "A terahertz electromagnetically induced transparency-like metamaterial for biosensing," in *2021 15th European Conference on Antennas and Propagation (EuCAP)*. IEEE, 2021, pp. 1–5.

[9] Q. Cassar, S. Caravera, G. MacGrogan, T. Bücher, P. Hillger, U. Pfeiffer, T. Zimmer, J.-P. Guillet, and P. Mounaix, "Terahertz refractive index-based morphological dilation for breast carcinoma delineation," *Scientific reports*, vol. 11, no. 1, pp. 1–16, 2021.

[10] G. Zhang, Y. Cao, J. Chen, P. Huang, W. Ge, and D. Hou, "Classification and identification of human colon cancer cell line in terahertz domain using t-sne," in *European Conference on Biomedical Optics*. Optical Society of America, 2019, p. 11073_45.

[11] F. Wahaia, I. Kašalynas, L. Minkevičius, C. D. C. Silva, A. Urbanowicz, and G. Valušis, "Terahertz spectroscopy and imaging for gastric cancer diagnosis," *Journal of Spectral Imaging*, vol. 9, 2020.

[12] S. Nourinovin, M. M. Rahman, R. C. Jones, M. P. Philpott, and A. Alomainy, "Impact of drug treatment on the electromagnetic properties of basal cell carcinoma cancer in the terahertz band," in *2022 16th European Conference on Antennas and Propagation (EuCAP)*. IEEE, 2022, pp. 1–4.

[13] R. Zhang, K. Yang, B. Yang, N. A. AbuAli, M. Hayajneh, M. Philpott, Q. H. Abbasi, and A. Alomainy, "Dielectric and double debye parameters of artificial normal skin and melanoma," *Journal of Infrared, Millimeter, and Terahertz Waves*, vol. 40, no. 6, pp. 657–672, 2019.

[14] B. C. Truong, H. D. Tuan, V. P. Wallace, A. J. Fitzgerald, and H. T. Nguyen, "The potential of the double debye parameters to discriminate between basal cell carcinoma and normal skin," *IEEE Transactions on Terahertz Science and Technology*, vol. 5, no. 6, pp. 990–998, 2015.

[15] E. Barroso, R. Smits, T. Bakker Schut, I. Ten Hove, J. Hardillo, E. Wolvius, R. J. Baatenburg de Jong, S. Koljenovic, and G. Puppels, "Discrimination between oral cancer and healthy tissue based on water content determined by raman spectroscopy," *Analytical chemistry*, vol. 87, no. 4, pp. 2419–2426, 2015.

[16] Y. B. Ji, J. M. Kim, Y. H. Lee, Y. Choi, D. H. Kim, Y.-M. Huh, S. J. Oh, Y. W. Koh, and J.-S. Suh, "Investigation of keratinizing squamous cell carcinoma of the tongue using terahertz reflection imaging," *Journal of Infrared, Millimeter, and Terahertz Waves*, vol. 40, no. 2, pp. 247–256, 2019.

[17] D. Li, Z. Yang, A. Fu, T. Chen, L. Chen, M. Tang, H. Zhang, N. Mu, S. Wang, G. Liang *et al.*, "Detecting melanoma with a terahertz spec-

MEMEA 2022, Conf MEMEA 2022, ConfID: 54994X

troscopy imaging technique," *Spectrochimica Acta Part A: Molecular and Biomolecular Spectroscopy*, vol. 234, p. 118229, 2020.

[18] Y. C. Sim, K.-M. Ahn, J. Y. Park, C.-S. Park, and J.-H. Son, "Temperature-dependent terahertz imaging of excised oral malignant melanoma," *IEEE Transactions on terahertz science and technology*, vol. 3, no. 4, pp. 368–373, 2013.

[19] C. Zhang, L. Liang, L. Ding, B. Jin, Y. Hou, C. Li, L. Jiang, W. Liu, W. Hu, Y. Lu *et al.*, "Label-free measurements on cell apoptosis using a terahertz metamaterial-based biosensor," *Applied Physics Letters*, vol. 108, no. 24, p. 241105, 2016.

[20] J. Singhal, S. Verma, S. Kumar, and D. Mehrotra, "Recent advances in nano-bio-sensing fabrication technology for the detection of oral cancer," *Molecular Biotechnology*, vol. 63, no. 5, pp. 339–362, 2021.

[21] Z. Zhang, H. Ding, X. Yan, L. Liang, D. Wei, M. Wang, Q. Yang, and J. Yao, "Sensitive detection of cancer cell apoptosis based on the non-bianisotropic metamaterials biosensors in terahertz frequency," *Optical Materials Express*, vol. 8, no. 3, pp. 659–667, 2018.

[22] X. Yan, M. Yang, Z. Zhang, L. Liang, D. Wei, M. Wang, M. Zhang, T. Wang, L. Liu, J. Xie *et al.*, "The terahertz electromagnetically induced transparency-like metamaterials for sensitive biosensors in the detection of cancer cells," *Biosensors and Bioelectronics*, vol. 126, pp. 485–492, 2019.

[23] Y. C. Sim, J. Y. Park, K.-M. Ahn, C. Park, and J.-H. Son, "Terahertz imaging of excised oral cancer at frozen temperature," *Biomedical optics express*, vol. 4, no. 8, pp. 1413–1421, 2013.

[24] J. Y. Park, Y. C. Sim, and J.-H. Son, "Frozen terahertz imaging of oral cancer," *Terahertz Biomedical Science and Technology*, p. 319, 2014.

[25] C. Jensen and Y. Teng, "Is it time to start transitioning from 2d to 3d cell culture?" *Frontiers in molecular biosciences*, vol. 7, p. 33, 2020.

[26] R. Zhang, K. Yang, Q. H. Abbasi, N. A. AbuAli, and A. Alomainy, "Impact of cell density and collagen concentration on the electromagnetic properties of dermal equivalents in the terahertz band," *IEEE Transactions on Terahertz Science and Technology*, vol. 8, no. 4, pp. 381–389, 2018.

[27] T. Zhang, R. Nazarov, A. P. Popov, P. S. Demchenko, A. V. Bykov, R. O. Grigorev, A. V. Kuzikova, V. Y. Soboleva, D. V. Zykov, I. V. Meglinski *et al.*, "Development of oral cancer tissue-mimicking phantom based on polyvinyl chloride plastisol and graphite for terahertz frequencies," *Journal of Biomedical Optics*, vol. 25, no. 12, p. 123002, 2020.

[28] M. Marques, A. Batista de Carvalho, A. Mamede, S. Rudić, A. Dopplapudi, V. García Sakai, and L. Batista de Carvalho, "Intracellular water as a mediator of anticancer drug action," *International Reviews in Physical Chemistry*, vol. 39, no. 1, pp. 67–81, 2020.

[29] X.-Y. Ke, V. W. L. Ng, S.-J. Gao, Y. W. Tong, J. L. Hedrick, and Y. Y. Yang, "Co-delivery of thioridazine and doxorubicin using polymeric micelles for targeting both cancer cells and cancer stem cells," *Biomaterials*, vol. 35, no. 3, pp. 1096–1108, 2014.

[30] B. E. Souza, S. Rudić, K. Titov, A. S. Babal, J. D. Taylor, and J.-C. Tan, "Guest–host interactions of nanoconfined anti-cancer drug in metal–organic framework exposed by terahertz dynamics," *Chemical Communications*, vol. 55, no. 27, pp. 3868–3871, 2019.

[31] C. O. Rodini, N. M. Lopes, V. S. Lara, and I. C. Mackenzie, "Oral cancer stem cells-properties and consequences," *Journal of Applied Oral Science*, vol. 25, pp. 708–715, 2017.

[32] M. M. Rahman, A. Hazan, J. L. Selway, D. S. Herath, C. A. Harwood, M. S. Pirzado, R. Atkar, D. P. Kelsell, K. J. Linton, M. P. Philpott *et al.*, "A novel mechanism for activation of gli1 by nuclear smo that escapes anti-smo inhibitors," *Cancer Research*, vol. 78, no. 10, pp. 2577–2588, 2018.

[33] A. Biddle, X. Liang, L. Gammon, B. Fazil, L. J. Harper, H. Emich, D. E. Costea, and I. C. Mackenzie, "Cancer stem cells in squamous cell carcinoma switch between two distinct phenotypes that are preferentially migratory or proliferative," *Cancer research*, vol. 71, no. 15, pp. 5317–5326, 2011.

[34] G. McIntyre, "Cell hydration as the primary factor in carcinogenesis: a unifying concept," *Medical hypotheses*, vol. 66, no. 3, pp. 518–526, 2006.

[35] M. Marques, A. Batista de Carvalho, A. Mamede, A. Dopplapudi, V. García Sakai, and L. Batista de Carvalho, "Role of intracellular water in the normal-to-cancer transition in human cells—insights from quasi-elastic neutron scattering," *Structural Dynamics*, vol. 7, no. 5, p. 054701, 2020.

[36] S. S. Jenifer Isabella, K. Sunitha, K. Magesh, S. P. Arjunan, and B. Pesala, "Investigation of formalin-fixed tissue optical characteristics in the range of 200–500 ghz using pulsed terahertz reflection spectroscopy to differentiate oral malignant, benign, and cyst," *Journal of Spectroscopy*, vol. 2022, 2022.

[37] C. S. Joseph, R. Patel, V. A. Neel, R. H. Giles, and A. N. Yaroslavsky, "Imaging of ex vivo nonmelanoma skin cancers in the optical and terahertz spectral regions optical and terahertz skin cancers imaging," *Journal of biophotonics*, vol. 7, no. 5, pp. 295–303, 2014.

[38] S. Takaoka, M. Iwase, M. Uchida, S. Yoshiba, G. Kondo, H. Watanabe, M. Ohashi, M. Nagumo, and S. Shintani, "Effect of combining epidermal growth factor receptor inhibitors and cisplatin on proliferation and apoptosis of oral squamous cell carcinoma cells," *International journal of oncology*, vol. 30, no. 6, pp. 1469–1476, 2007.

[39] Y. Hiraishi, T. Wada, K. Nakatani, I. Tojyo, T. Matsumoto, N. Kiga, K. Negoro, and S. Fujita, "Egfr inhibitor enhances cisplatin sensitivity of oral squamous cell carcinoma cell lines," *Pathology & Oncology Research*, vol. 14, no. 1, pp. 39–43, 2008.

[40] L. Ma, H. Yan, and Q. Zhou, "Ag1478 inhibits the migration and invasion of cisplatin-resistant human lung adenocarcinoma cells via the cell cycle regulation by matrix metalloproteinase-9," *Oncology letters*, vol. 8, no. 2, pp. 921–927, 2014.

[41] M. Marques, A. B. De Carvalho, V. G. Sakai, L. Hatter, and L. B. De Carvalho, "Intracellular water–an overlooked drug target? cisplatin impact in cancer cells probed by neutrons," *Physical Chemistry Chemical Physics*, vol. 19, no. 4, pp. 2702–2713, 2017.